Performace Of Print Masks Using Image Quality Measurements

J. William Boley, ChenChao Shou, George T.-C. Chiu; Purdue University, West Lafayette, IN/USA

Abstract

With the increase in applications of inkjet functional printing in recent years, the higher throughput associated with multiple nozzle arrays is necessary for large scale production. This provides the motivation for designing print masks that can maximize the quality of inkjet printed devices rather than minimize the number of print artifacts detectable by the human eye. The current study builds upon earlier work by introduing a new drop coalescence cost function and by measuring the performance of print masks resulting from the Print Mask Direct Binary Search via image quality metrics including image mottle, raggedness, and fill. Three print masks of differing expected quality are generated and used to print rectangular solid fills. Overall, the results from the printed samples are in agreement with the expected performance of each of the three print masks. Discrepencies from image size and image variability show limitations in the current study. Future work will involve measuring the performance of the print mask by measuring the performance of the device.

Introduction

For more than a decade studies [1–3] have shown that print masks can be designed to alleviate print artifacts in inkjet printed images by using the ability to simultaneously address any combination of nozzles in multi-nozzled printheads.

Early work [1] in this area has included the application of halftoning techniques and super-smooth dithering matrices. These tools were used to design two-pass print masks that eliminated banding and forced ink migration to spatial frequencies above the human perceivable range. Subsequent work [2] cast print mask design as a constrained optimization problem and developed a general mathematical framework to allow for the application of different print modes, including multiple levels and multiple drops per pixel.

With the increase in applications of inkjet functional printing in recent years [4, 5], the higher throughput associated with multiple nozzle arrays is necessary for large scale production. This provides the motivation for designing print masks that can maximize the quality of inkjet printed devices rather than minimize the number of print artifacts detectable by the human eye.

A study recently proposed a print mask design [6] that modified the direct binary search algorithm to obtain a print mask which minimized a cost function. With functional printing applications in mind, the researchers utilized the print mask direct binary search (PMDBS) to minimize a cost function considering occurrence of coalescence and drop placement error, as both of these factors have the potential to affect device performance (e.g.s, open or short circuits or non-uniform illumination in printed displays).

This study builds upon the work by Boley et al. [6] by a new cost function for drop coalescence and by measuring the performance of print masks resulting from the PMDBS via image quality metrics. First, an overview of the PMDBS is presented, including the constraint used to avoid passes with no nozzle firing, the drop placement cost function, and a modification of the coalescence cost function. Next, the selection of quality metrics used in this study are discussed. Then the experimental procedure for obtaining the drop placement and drop radius distributions is provided. Following, the print quality metrics resulting from solid fill rectangles printed by three different print masks designed by the PMDBS are provided and discussed. Last is a discussion of the conclusions from this work.

Overview of the PMDBS

The purpose of this section is to provide the bare necessities of the PMDBS used for this study, namely the constraint invoked and cost functions to be minimized. A more complete description of the algorithm may be found in [6]. In general, the PMDBS goes as follows. Given a print mode, a random initial admissible print mask (*PM*) is generated and its associated cost function evaluated. Next, the initial *PM* is copied and scanned in raster fashion. For each element scanned the algorithm loops through the set $\{1,2,\ldots,n\}$, where n is the total number of passes in the print mode, and computes the cost associated with the *PM* if the scanned element were changed to one of the elements in $\{1,2,\ldots,n\}$. If the cost decreases and the resulting *PM* satisfies the constraint(s), then the change is made to the copy of the initial *PM*, the cost function is recorded, and scanning is continued until the last element in the initial *PM* is reached. Once scanning is complete, the resulting *PM* is compared to the *PM* prior to scanning. If they are the same, then the algorithm has converged and the resulting *PM* is a local minimizer of the cost function. Otherwise, the algorithm sets the resulting *PM* to be the initial *PM* and the algorithm scans again. Since the result of the PMDBS is a local minimizer, the algorithm can be run multiple times to obtain a better sense of a global minimizer. The remainder of this section will discuss the constraint and cost functions used for this study.

Avoiding Passes With No Nozzle Firings

In order to reduce energy consumption with unused stage motion and to decrease nozzle idle time the following constraint is applied so that nozzle firing occurs during each pass [6].

$$\bigcup_{i,j}\{PM(i,j)\} = \{1,2,\ldots,n\}; \tag{1}$$

where $i = 1,2,\ldots,p_1$, $j = 1,2,\ldots,p_2$, p_1 is the number of rows in *PM*, and p_2 is the number of columns in *PM*.

Drop Placement Cost Function

As described in [6], let γ_{dp} be a weighting on the drop placement, $\varepsilon_{q_1 q_2 w_{dp}}$ be the relative biased drop placement error between the nozzle responsible for printing image pixel (q_1,q_2) and the nozzle responsible for printing neighbor pixel w_{dp}, where w_{dp} is

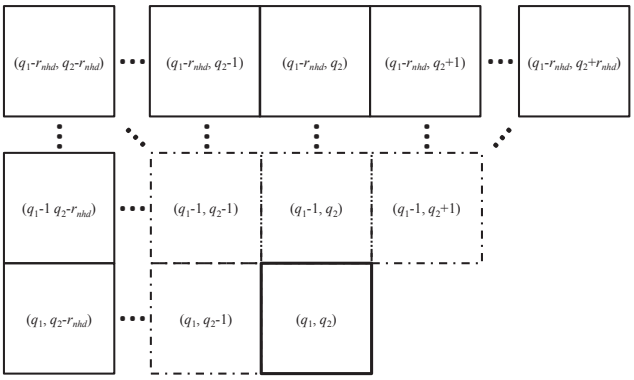

Figure 1. *Neighborhood of Interest for Image Pixel* (q_1, q_2).

an image pixel contained in the smaller neighborhood nhd_{dp} of (q_1, q_2) denoted by dashed lines in Fig. 1. Let $\sigma x^2_{q_1q_2}$ and $\sigma y^2_{q_1q_2}$ be the variance of the drop placement associated with the nozzle that prints image pixel (q_1, q_2) in the print-head scan and media advance directions, respectively. Let $\sigma x^2_{w_{dp}}$ and $\sigma y^2_{w_{dp}}$ be the variance of the drop placement error associated with the nozzle that prints neighbor w_{dp} in the print-head scan and media advance directions, respectively. Then the image pixel (q_1, q_2) and neighbor w_{dp} dependent cost function for drop placement is

$$f_{dp}(q_1, q_2, w_{dp}) = \gamma_{dp} \sum_{w_{dp} \in nhd_{dp}} \left(\varepsilon_{q_1q_2w_{dp}} + \sqrt{\sigma x^2_{q_1q_2} + \sigma y^2_{q_1q_2} + \sigma x^2_{w_{dp}} + \sigma y^2_{w_{dp}}} \right). \quad (2)$$

To clarify the notation, it should be noted that given a print mode and a *PM*, the nozzle responsible for depositing ink onto each image pixel is determined [7]. It should also be noted that for a given print mode the pixel resolution and the drop deposition time are known as well [6, 7]. Therefore, when we say that something depends on the image pixel for a given *PM* and print mode, it is equivalent to saying that it depends on the nozzle assigned to the image pixel as well as the time of deposition and physical location of said pixel.

Coalescence Cost Function

There are a couple of modifications to the coalescence cost function that this paper is making. The first is an increase in neighborhood size for each image pixel (q_1, q_2). The second is the cost function itself.

Previously, [6] only considered the the dashed-line neighborhood in Fig. 1. However, due to drop placement error and the fact that the drop radius is typically larger than the image resolution, a larger neighborhood should be considered.

The coalescence cost function in [6] is a measure of how early adjacent drops are deposited relative to a minimum waiting time for a prescribed allowable occurrence of coalescence. However, it is easier to interpret a cost function that reports the probability that a drop deposited onto an image pixel will coalesce with one of its neighbors.

Let r_{nhd} be the maximum number of pixels away from any image pixel that has a non-zero probability of coalescence for any nozzle pair combination. Let γ_c be a weighting on drop coalescence and w_c an image pixel contained in the large neighborhood nhd_c of radius r_{nhd} shown in Fig. 1. Assuming coalescence among each neighbor to be independent, the image pixel (q_1, q_2) and neighbor w_c dependent cost function for drop coalescence is a weighting on the probability that the drop deposited onto image pixel (q_1, q_2) will coalesce with any of its neighbors in nhd_c, written as

$$f_c(q_1, q_2, w_c) = \gamma_c \left(1 - \prod_{w_c \in nhd_c} (1 - P_{q_1q_2w_c}) \right); \quad (3)$$

where $P_{q_1q_2w_c}$ is the probability that the drop deposited onto image pixel (q_1, q_2) will coalesce with a drop deposited onto image pixel w_c.

The cost fuction for a given *PM* can now be written as

$$f = \sum_{Q} \left(f_{dp}(q_1, q_2, w_{dp}) + f_c(q_1, q_2, w_c) \right); \quad (4)$$

where Q is the set of all image pixels.

Image Quality Metrics Used

There are many attributes given in [8, 9] that measuere the quality of a given image. Rather than including all measures, three attributes naturally thought to be indicative of device performance were chosen from [8]. These three image quality attributes are mottle, raggedness, and fill. This section gives a brief description of these attributes and discusses how they can relate to functional printing.

Mottle

Mottle as defined in [8] as irregular spatial patterns with frequencies less than 0.4 cycles per *mm* in every direction. To compute mottle, the region of interested as defined by [8] is divided into at least 100 uniform, non-overlapping square tiles. The mottle is then obtained by taking the standard deviation of the average optical density over all tiles. Further investigation has shown that mottle can be reported in terms of the grayscale value (GSV), mottle is a function of the tile size, and that mottle is an indicator of the occurrence of coalescence within an image [10]. Therefore, the mottle method proposed in [10] has been chosen to measure *PM* performance in this paper.

Raggedness

Raggedness is described in [8] as the standard deviation of the residual error perpendicular to the best fit edge threshold. This attribute was chosen because the raggedness of a line can affect the performance of a printed device (e.g., two adjacent conductive traces in close proximity are less likely intersect if they have low raggedness).

Fill

The third attribute used in this study is fill. It is defined [8] as the ratio of the area within the region of interest that has a relative reflectance of at least 75% to the total area of the region of interest. Fill is a measure of image homogeneity, which is important in printed devices such as displays [11].

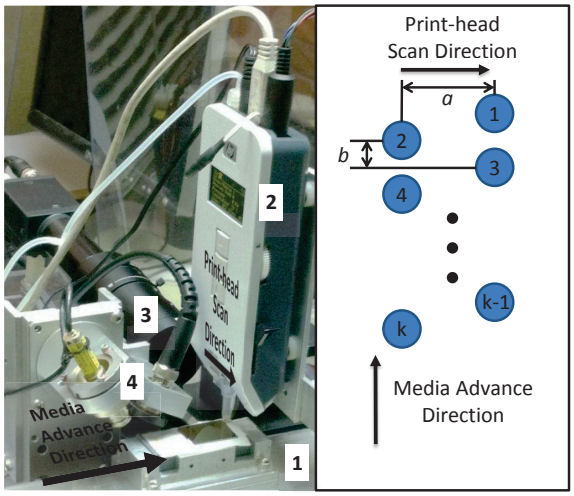

Figure 2. *(Left) Photograph of inkjet system consisting of 1.Motorized XY stage, 2.Thermal drop ejector, 3.CCD camera, and 4.Laser sample registration system. (Right) Schematic of the print-head geometry(Drop into the page). Directions are labeled in each to show relative orientation.*

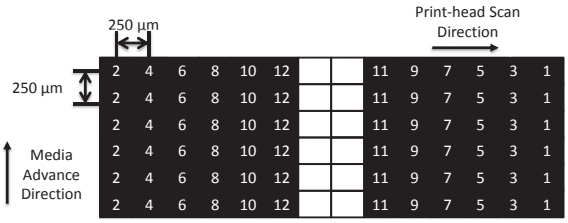

Figure 3. *Input image designed for obtaining print-head nozzle locations and drop placement and radius distributions.*

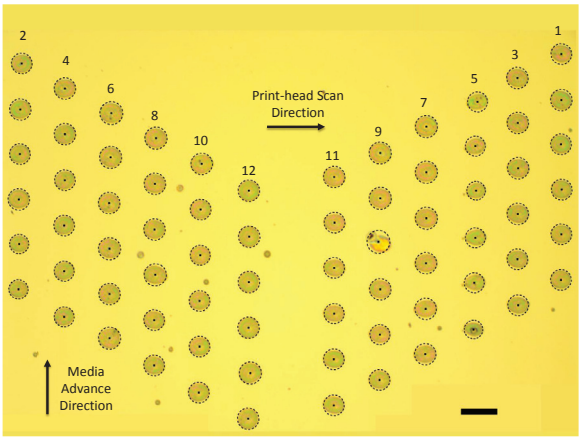

Figure 4. *Printed image resulting from input image Fig. 3. Each column is labeled with its corresponding nozzle. Directions are labeled to aid in orientation. Scale bar is 200 µm.*

Procedures

The purpose of this section is to describe the inkjet system used in the study, provide the methods used for characterizing the drop placement and drop radius distributions, and to briefly explain how the model for drop coalescence is obtained.

System Description

The inkjet system used for conducting experiments for this study is shown in Fig. 2. The motion system consists of an XY stage (Anorad-XKY-C-150-AAA0), which uses DC servo driven permanent magnet epoxy core linear motors for independent motion in both axes. The motion is controlled by a SPiiPlus Series Stand Alone controller, with linear encoder feedback of $0.5\mu m$.

The drop ejection system used is provided by HP®, utilizes thermal inkjet technology, and offers print-heads with $k = 10, 12$, or 16 nozzles. The nozzle orifices range from $8.0\mu m$ to $80.0\mu m$. The print-head used for all experiments had $k = 12$ nozzles with a nominal orifice diameter of $67\mu m$.

The system also includes a Sony® XC-ST50 charged coupled device (CCD) camera for viewing during deposition and a laser sample registration system for mapping out edges of a substrate [12].

All experiments conducted involved printing an $100mM$ solution of Pd hexadecanethiolate thiolate in toluene, which has previously been used to print metal interconnects and surface-enhance Raman scattering substrates [13]. The substrates employed for the experiments were Si wafers. All images were printed with unidirectional printing at a print-head scan speed of $1mm/s$, a media advance speed of $1mm/s$, a print-head return speed of $45mm/s$, and a standoff distance of approximately $250\mu m$ from the substrate. An Olympus BX-60 microscope was used to capture printed samples.

Characterizing Drop Placement and Drop Radius Distributions

Initial experiments were conducted in order to find the drop placement and drop radius distributions, the nozzle column spacing a, the nozzle resolution b, and the coalescence neighborhood radius r_{nhd} required for the PMDBS. The image shown in Fig. 3 is the input image designed to obtain the aforementioned data. Black pixels correspond to pixels with ink and white corresponds to ones without ink. Each black pixel is labeled with the nozzle responsible for depositing ink onto it.

The resulting printed image, Fig. 4, was analyzed using MATLAB to find the centroid and radius of each drop. The drop centroids were found using an algorithm by Bernal et al. [14] and are shown in Fig. 4 (black squares) superimposed onto the printed image. The drop radii were found using a simple least squares algorithm by Chaudhuri [15]. The black dashed-line circles featured in Fig. 4 were generated using the centroid and radius for each drop obtained from the analysis.

In order to obtain the distributions a 3×3 array of the input image in Fig. 3 was first printed. Secondly, the centroid and radius for each drop in the printed image were obtained. From here the the relative drop placement distributions for each nozzle (see Fig. 5(a)) and the radius distribution (see Fig. 5(b)) were easily attained. Taking the average relative position in the print-head scan direction over all drop placement distributions resulted in a nozzle column spacing of $a = 266.01\mu m$. Using MATLAB's *polyfit* for the mean of the relative drop placement distribution in the media advance direction for each nozzle resulted in a nozzle resolution

of $b = 70.25\mu m$. Considering the worst case scenerio, the coalescence neighborhood radius is found to be $r_{nhd} = 3$ pixels.

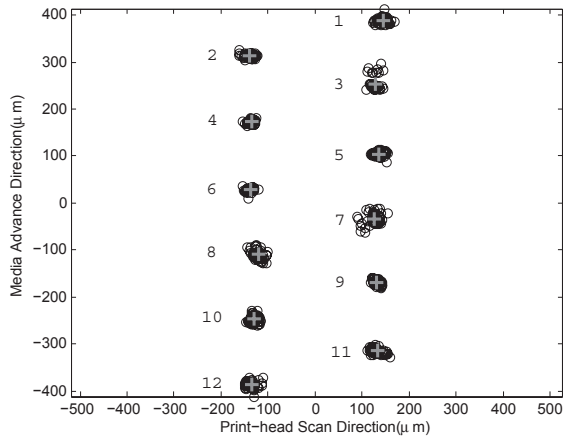

(a) Experimentally obtained relative drop placement distributions (black circles) for each nozzle and their corresponding mean value (gray plus signs). Each distribution and mean is labeled by its corresponding nozzle.

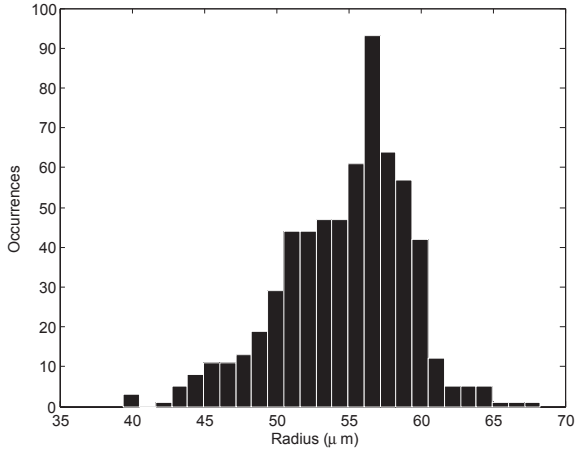

(b) Histogram of experimentally obtained drop radii including all nozzle for all trials. Data outside of three standard deviations have been removed.

Figure 5. *Experimentally obtained drop placement and radius distributions.*

Coalescence Modeling

A lookup table was generated that contains time and probability of coalescence vectors for each nozzle pair combination for each possible neighbor, $w_c \in nhd_c$. The time and probability of coalescence vectors were obtained using the stochastic model of coalescence on non-porous substrates described in [16,17], which considers coalescence to occur when the wetted areas of two deposited drops intersect, resulting in the merging of the two drops into one drop via surface tension. The locations and initial volumes of the deposited drops are random, making coalescence a stochatic event. An optimal combination between two modes of sessile drop evaporation (constant contact angle and constant contact radius) [17] of the initially deposited drop is the physical phenomenon causing the event of coalescence to change with time.

Summary of PMDBS Cost Functions

Pass Number	Coalescence	Drop Placement(*mm*)
2	34.26	43.03
3	9.82	43.33
4	4.78	42.89

Image Quality Results and Discussion

The print mode parameters constant for all image quality experiments are as follows:

- Print-head scan speed, $1mm/s$
- Unidirectional printing
- Media advance speed, $1mm/s$
- Print-head return speed, $45mm/s$
- Nozzle resolution, $b = 70.25\mu m$
- Image resolution, $70.25\mu m/pixel$
- Ink, $100mM$ solution of Pd hexadecanethiolate in toluene
- Substrate, Si wafers
- Distance between nozzle columns, $a = 266.01\mu m$
- Print Mask size, 4 rows $\times$ 4 columns
- Radius of coalescence neighborhood, $r_{nhd} = 3$ pixels
- Image, 15×8 filled rectangle.

The PMDBS was run 20 times for three different pass numbers ($n = 2,3,4$) with $\gamma_c = 1$ and $\gamma_c = 0.001$. The *PM* resulting in the lowest cost function for each case was

$$PM_2 = \begin{pmatrix} 1 & 2 & 1 & 2 \\ 1 & 2 & 2 & 1 \\ 2 & 1 & 2 & 1 \\ 2 & 1 & 1 & 2 \end{pmatrix}, PM_3 = \begin{pmatrix} 1 & 2 & 1 & 3 \\ 1 & 2 & 3 & 1 \\ 3 & 1 & 3 & 2 \\ 3 & 1 & 2 & 1 \end{pmatrix},$$

and

$$PM_4 = \begin{pmatrix} 4 & 2 & 4 & 2 \\ 3 & 1 & 2 & 4 \\ 2 & 4 & 1 & 4 \\ 1 & 3 & 4 & 1 \end{pmatrix};$$

where the subscript for each PM_i denotes the number of passes.

Results and Discussion

The summary of the resulting cost functions for each print mask is shown in Table 1. Upon inspection of the resulting cost functions, it is clear that the coalescence cost function varies more than the drop placement cost function across the three print masks with the largest change occurring between pass numbers 2 and 3. This is in agreement with the printed images as it appears that the largest reduction in occurrence of coalescence happens between pass numbers 2 and 3. Following the conversion of the images in Fig. 6 to grayscale values, image analysis was performed to exctract mottle, raggedness, and fill.

Mottle was obtained for tile sizes ranging from $2\mu m$ up to $152\mu m$ as it is known that mottle is sensitive to tile size [10]. The results for mottle are shown in Fig. 7. In comparing mean

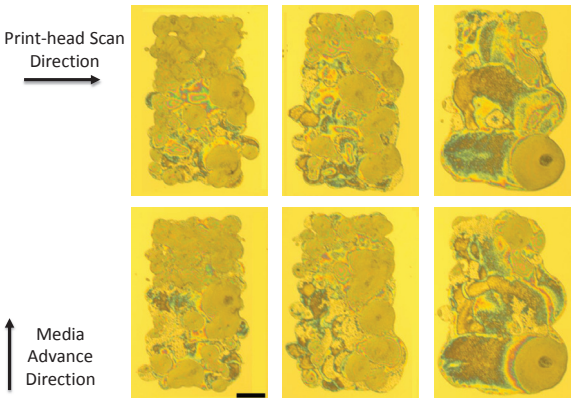

Figure 6. *Images printed using PM_4(Left Column), PM_3(Middle Column), and PM_1(Right Column). The calibration bar is $200\mu m$.*

mottle values for each *PM* to the printed images it is clear that mottle indeed increases with coalescence as observed by Jones et al. [10] and furthermore that the same trend visible between the coalescence cost functions and the printed images can be seen in the mean mottle values. In only one case (tile size of $112\mu m$) is the mean mottle for PM_3 smaller than that for PM_4. The mottle variability across images also changes with tile size. Further investigation shows that tile sizes smaller than $32\mu m$ (32 pixels per tile) still show a significant mottle difference between PM_4 and PM_3, which is in line with observations of the printed images.

The results of raggedness (in μm) and fill are summarized in Table 2. Comparing the mean value of these results does indeed show agreement with the result from mottle from viewing the printed images and from the cost functions resulting from the PMDBS. However, the sensitivity is not as large compared to the lower tile sizes of mottle. The variability across images makes it difficult to use raggedness or fill as a comparison between PM_3 and PM_4 or PM_2.

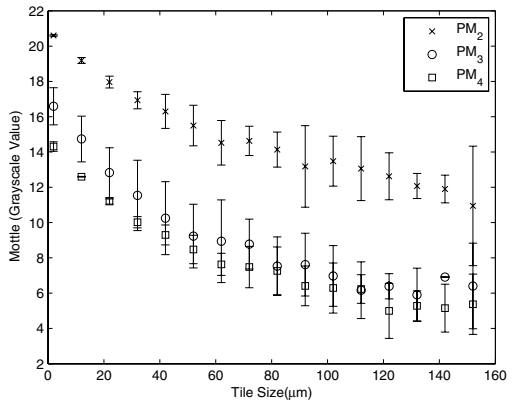

Figure 7. *Mean value of mottle of the two images printed for each print mask. Length of errorbars is two standard deviations.*

Limitations and Future Work

Overall, the results from the printed samples and the image quality measurements are in agreement with the expected performance of each of the three print masks. However, there seems to be some discrepencies coming from image variability for all image measurements and tile size for mottle. These discrepencies are most likely due to the limited image size. In order to obtain a more sensitive comparison of print mask perfomance, future work will be to measure the performance of the actual printed device (e.g., the resistivity of a printed conductor). Due to limited memory space on the drop ejection controller for nozzle configurations, the maximum number of passes was 4. Current work is being done to increase this number to show results of higher performing print masks.

Summary of Image Quality Results

	Top Image		Bottom Image	
Pass Number	Raggedness	Fill	Raggedness	Fill
2	35.68	0.84	34.31	0.87
3	25.37	0.88	38.41	0.93
4	30.44	0.92	26.77	0.91

Conclusions

In closing, the proposed PMDBS is in agreement with the quality of the images and the resulting image quality metrics that were proposed. Discrepencies most likely from image size and variability across images for a given *PM* show the need for a more sensitive comparison of print mask performance. Future work involves comparing print mask performance by comparing the resulting devices' performance. Future work also includes increasing the number of nozzle configurations that can be loaded onto the drop ejection controller so that larger images can be printed and higher quality print masks can be used.

Acknowledgments

The authors would like to thank the HP Corvalis team for their support with troubleshooting the drop ejection device. We would also like to thank Dr. Timothy Fisher and his students, particularly Stephen Hodson and Guoping Xiong for their assistance with imaging the printed samples and obtaining the ink and substrates used for the experiments.

References

[1] Yen, J., Lin, Q., and Wong, P., 1999. Print masks for inkjet printers. US Patent 5,992,962.

[2] Yen, J., Carlsson, M., Chang, M., Garcia, J., and Nguyen, H., 2000. "Constraint solving for inkjet print mask design". *Journal of Imaging Science and Technology,* **44**(5), SEP-OCT, pp. 391–397.

[3] Boley, W., Bhuvana, T., Hines, B., Sayer, R. A., Chiu, G., Fisher, T. S., Bergstrom, D., Reifenberger, R., and Kulkarni, G. U., 2009. "Inkjet Printing Involving Palladium Alkanethiolates and Carbon Nanotubes Functionalized with Single-Strand DNA". pp. 824–827. 25th International Conference on Digital Printing Technologies, Louisville, KY, SEP 20-24.

[4] Calvert, P., 2001. "Inkjet printing for materials and devices". *Chemistry of Materials,* **13**(10), OCT, pp. 3299–3305.

[5] de Gans, B., Duineveld, P., and Schubert, U., 2004. "Inkjet printing of polymers: State of the art and future developments". *ADVANCED MATERIALS,* **16**(3), FEB 3, pp. 203–213.

[6] Boley, J. W., and Allebach, Jan P., C. G. T.-C., 2011. "Direct Binary Search for Print Mask Design in Inkjet Printing". 27th International Conference on Digital Printing Technologies, Seattle, WA, NOV 2-7.

[7] Boley, J., and Chiu, G., 2010. "Print Mask Design for Maximum Throughput Subject to Print Quality Constraints". 26th International Conference on Digital Printing Technologies, Austin, TX, SEP 19-23.

[8] ISO/IEC/ 13660 draft standard, information technology office equipment - measurement of image quality attributes for hardcopy output - binary monochrome text and graphic images.

[9] Shaw, R., 1997. "Image Quality Considerations for Printing Digital Photographs". 13th International Conference on Digital Printing Technologies, Minneapolis, MN, OCT 2-6.

[10] Jones, N., Sargeant, S. J., and Sargeant, K., 1998. "Characterizing and Modeling Coalescence in Inkjet Printing". 14th International Conference on Digital Printing Technologies, Toronto, Ontario, Canada, OCT 18-23.

[11] Soltman, D., Smith, B., Kang, H., Morris, S. J. S., and Subramanian, V., 2010. "Methodology for Inkjet Printing of Partially Wetting Films". *Langmuir,* **26**(19), OCT 5, pp. 15686–15693.

[12] Post, N. J., 2007. "Precision Micro-Deposition of Functional Layers Using Inkjet Drop-On-Demand and Applications to the Functionalization of Microcantilever Sensors". MS Thesis, Purdue University, West Lafayette, IN, August.

[13] Bhuvana, T., Boley, W., Radha, B., Dolash, B. D., Chiu, G., Bergstrom, D., Reifenberger, R., Fisher, T. S., and Kulkarni, G. U., 2010. "Inkjet printing of palladium alkanethiolates for facile fabrication of metal interconnects and surface-enhanced Raman scattering substrates". *Micro & Nano Letters,* **5**(5), OCT, pp. 296–299.

[14] Bernal, E., Allebach, J. P., and Pizlo, Z., 2007. "Improved pen alignment for bidirectional printing". *Journal of Imaging Science and Technology,* **51**(1), pp. 1–22.

[15] Chaudhuri, D., 2010. "A simple least squares method for fitting of ellipses and circles depends on border points of a two-tone image and their 3-D extensions". *PATTERN RECOGNITION LETTERS,* **31**(9), JUL 1, pp. 818–829.

[16] Boley, J., Sayer, R., and Chiu, G., 2011. "Stochastic Modelling of Drop Coalescence on Non-Porous Substrates for Inkjet Applications". Proceedings of the 2011 ASME Dynamic Systems and Control Conference, Arlington, VA, OCT 31 - NOV 2.

[17] "To be published".

Author Biography

J. William Boley received a BS with a double major in Mechanical Engineering and Mathematics as well as an MS in Mechanical Engineering from the University of Kentucky. He is currently pursuing a Ph.D. in the School of Mechanical Engineering at Purdue University. He is a member of IS&T, IEEE, and ASME.